Fast and Accurate Analysis of Reflector Antennas with Phased Array Feeds Including Multiple Reflections between Feed and Reflector

Fast and Accurate Analysis of Reflector Antennas with Phased Array Feeds including Multiple Reflections between Feed and Reflector

O. A. Iupikov, *Student Member, IEEE*, R. Maaskant, *Senior Member, IEEE*, M. V. Ivashina, *Senior Member, IEEE*, A. Young, *Member, IEEE*, and P. S. Kildal, *Fellow, IEEE*

***Abstract*—Several electrically large Phased Array Feed (PAF) reflector systems are modeled to examine the mechanism of multiple reflections between parabolic reflectors and low- and high-scattering feeds giving rise to frequency-dependent patterns and impedance ripples. The PAF current is expanded in physics-based macro domain basis functions (CBFs), while the reflector employs the Physical Optics (PO) equivalent current. The reflector-feed coupling is systematically accounted for through a multiscattering Jacobi approach. An FFT expands the reflector radiated field in only a few plane waves, and the reflector PO current is computed rapidly through a near-field interpolation technique. The FEKO software is used for several cross validations, and the convergence properties of the hybrid method are studied for several representative examples showing excellent numerical performance. The measured and simulated results for a 121-element Vivaldi PAF, which is installed on the Westerbork Synthesis Radio Telescope, are in very good agreement.**

***Index Terms*—phased array feeds, radio astronomy, method of moments, characteristic basis function method, physical optics.**

I. Introduction

FOCAL plane arrays can be used to form multiple reflector beams covering a wide field-of-view (FoV) and large bandwidth. Among these feeds, one can distinguish between a cluster of horns yielding one beam per feed [1], [2], and the more densely packed beamforming array antennas commonly referred to as Phased Array Feeds (PAFs) capable of providing a continuous FoV of simultaneous beams. Examples that benefit from these technologies are radars and terrestrial communications; while since recently, PAFs have also been developed for astronomical and geoscientific instruments, as well as for commercial satellite communication terminals [3]–[6]. Thanks to their electronic beamforming capabilities, these new systems potentially enable much faster studies of the Earth and Space than currently possible and are an attractive alternative to bulky mechanically beam steered antennas.

O. A. Iupikov, R. Maaskant, M. V. Ivashina, and P. S. Kildal are with the Signals and Systems Department of the Chalmers University of Technology, Gothenburg, Sweden, e-mail: oleg.iupikov@chalmers.se, rob.maaskant@chalmers.se, marianna.ivashina@chalmers.se, per-simon.kildal@chalmers.se.

A. Young is with the Electronic and Electrical Engineering Department of the Stellenbosch University, Stellenbosch, South Africa, e-mail: ayoung@sun.ac.za.

This work is financed by Swedish VR and VINNOVA grants and the SKA South Africa, the South African Research Chairs Initiative of the Department of Science and Technology (DST), and the National Research Foundation (NRF).

Manuscript received April xx, 20xx; revised January xx, 20xx.

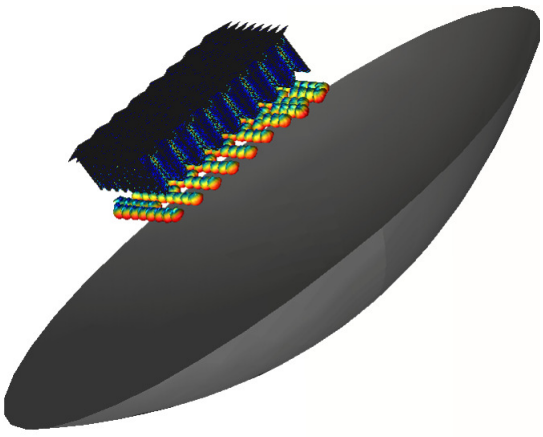

Fig. 1. Reflector antenna and a Phased Array Feed (PAF) system.

The characterization of feeds in unblocked reflectors and on-axis beams can be handled by the traditional spillover, illumination, polarization and phase subefficiency factors defined for rotationally symmetric reflectors in [7], and be extended to include excitation-dependent decoupling efficiencies of PAFs [8], [9]. The present paper investigates the effects of aperture blockage and multiple reflections on the system performance in a more generic fashion than in [10] and [11] for rotationally symmetric antennas.

An accurate analysis of these PAF systems, which include an array of many closely-spaced antenna elements and an electrically large reflector (see e.g. Fig. 1), requires a modeling approach for the entire feed-reflector structure accounting for the array mutual coupling and the multiple scattering effects between the reflector and the feed, whose aperture diameter can be in the order of several wavelengths for multi-beam applications [12], [13]. These effects give rise to a ripple in the antenna impedance and radiation characteristics over frequency leading to impedance mismatch effects and a periodically perturbed beam shape [14]–[18]. The level of these variations depends on several factors related to the reflector geometry and feed design, among which the blockage area of the reflector aperture caused by the feed, the antenna array scattering characteristics [19, Sec. 2.2], the weighting coefficients of the beamforming network, and the presence of the (metal) structure in the vicinity of the feed [20]. In order to solve these challenging problems, a method is needed that is fast and physically-insightful for understanding how the EM coupling mechanism between the PAF and reflector antenna

impacts the overall system performance.

During the last decades, a number of analytical and numerical techniques have been developed to model feed-reflector interaction effects. For example, in [10] the multiscattered field is approximated by a geometric series of on-axis plane wave (PW) field scattered by the antenna feed due to an incident PW at each iteration, where the amplitudes of these PWs are expressed analytically for a given reflector geometry. This method is very fast and insightful, while MoM-level accuracy can be achieved for single-horn feeds, but not for array feeds as demonstrated in this paper. An alternative approach is to use more versatile, though more time-consuming, hybrid numerical methods combining Physical Optics or Gaussian beams for the analysis of reflectors with MoM and/or Mode Matching techniques for horn feeds [21], [22]. The recent article [23] has introduced the PO/Generalized-Scattering-Matrix approach for solving multiple domain problems, and has shown its application to a cluster of a few horns. This approach is generic and accurate, but may require the filling of a large scattering matrix for electrically large PAFs and/or multifrequency front-ends (MFFEs) that often have an extended metal structure [17]. Other hybrid methods, which are not specific for solving the present type of problems, make use of field transformations, field operators, multilevel fast multipole approaches (MLFMA), and matrix modifications [24]–[27].

Recently, a Krylov subspace iterative method has been combined with an MBF-PO approach for solving feed-reflector problems [28], and complementary to this, an iteration-free CBFM-PO approach has been presented by Hay, where a modified reduced MoM matrix for the array feed is constructed by directly accounting for the reflector [16].

Among the above methods, the iterative methods have shown to be most useful for gaining insight in the feed-reflector multiscattering effects. In the present paper, we therefore employ the Jacobi iterative approach as a simplified version of the full orthogonalization method (FOM [28]), and combine it with an CBFM-PO approach enhanced by field expansion (see also [18]) and interpolation techniques. The method is shown to converge within a few iterations.

The paper is arranged as follows: first, the numerical approach is formulated and then validated through a few representative examples, after which the field expansion and interpolation techniques are described along with a numerical accuracy and efficiency assessment; second, the performance and the multiscattering mechanism between electrically large reflector antennas and several fundamentally different types of feeds, including single-pixel horn feeds as in practical MFFEs, and 121-element PAFs of dipoles and tapered slot Vivaldi antennas are studied for different port termination schemes. The predicted system sensitivity is in very good agreement with the measurements of a single horn and Vivaldi PAF system feeding one of the 25-m Westerbork Synthesis Radio Telescope reflector antennas [29].

II. Iterative CBFM-PO Formulation

The below proposed iterative CBFM-PO approach is based upon the Jacobi method for solving a system of linear equations in an iterative manner [30], [31].

Suppose the Method of Moments (MoM) matrix equation of the entire antenna system comprised of both the parabolic reflector and the antenna feed is given by

$$\mathbf{Z}\mathbf{I} = \mathbf{V}, \tag{1}$$

where the elements of the $K \times K$ MoM matrix $\mathbf{Z}$ and $K \times 1$ excitation vector $\mathbf{V}$ are computed as

$$Z_{pq} = \langle \boldsymbol{f}_p, \boldsymbol{E}^{\mathrm{s}}(\boldsymbol{f}_q)\rangle, \qquad V_p = -\langle \boldsymbol{f}_p, \boldsymbol{E}^{\mathrm{i}}\rangle \tag{2}$$

for $p, q = 1, 2, \ldots K$. Furthermore, $\boldsymbol{f}_{p,q}$ are the K basis/test functions for the current/field (Galerkin method); $\boldsymbol{E}^{\mathrm{i,s}}$ is the incident/scattered electric field, and $\langle \boldsymbol{a}, \boldsymbol{b}\rangle = \iint_{S_a \cap S_b} [\boldsymbol{a} \cdot \boldsymbol{b}]\, \mathrm{d}S$ is the symmetric product, where S_a and S_b are the supports of the vector functions $\boldsymbol{a}$ and $\boldsymbol{b}$, respectively. The expansion coefficient vector is given by $\mathbf{I} = [I_1, \ldots I_K]^T$, where T denotes the transposition operator.

To allow for a multiscattering analysis between the feed and reflector, the MoM matrix equation in (1) is first partitioned into matrix blocks as

$$\begin{bmatrix} \mathbf{Z}^{\mathrm{rr}} & \mathbf{Z}^{\mathrm{rf}} \\ \mathbf{Z}^{\mathrm{fr}} & \mathbf{Z}^{\mathrm{ff}} \end{bmatrix} \begin{bmatrix} \mathbf{I}^{\mathrm{r}} \\ \mathbf{I}^{\mathrm{f}} \end{bmatrix} = \begin{bmatrix} \mathbf{V}^{\mathrm{r}} \\ \mathbf{V}^{\mathrm{f}} \end{bmatrix} \tag{3}$$

where $\mathbf{Z}^{\mathrm{rr}}$ and $\mathbf{Z}^{\mathrm{ff}}$ are the MoM matrix self-blocks of the reflector and feed, respectively[1], and $\mathbf{V}^{\mathrm{r}}$ and $\mathbf{V}^{\mathrm{f}}$ are the corresponding excitation vectors. The matrix $\mathbf{Z}^{\mathrm{rf}} = (\mathbf{Z}^{\mathrm{fr}})^T$ contains the mutual reactions involving the basis functions on the feed and reflector. The unknown current expansion coefficient vectors are denoted by $\mathbf{I}^{\mathrm{r}}$ and $\mathbf{I}^{\mathrm{f}}$. Next, Eq. (3) is written as

$$\left(\begin{bmatrix} \mathbf{Z}^{\mathrm{rr}} & \mathbf{0} \\ \mathbf{0} & \mathbf{Z}^{\mathrm{ff}} \end{bmatrix} + \begin{bmatrix} \mathbf{0} & \mathbf{Z}^{\mathrm{rf}} \\ \mathbf{Z}^{\mathrm{fr}} & \mathbf{0} \end{bmatrix} \right) \begin{bmatrix} \mathbf{I}^{\mathrm{r}} \\ \mathbf{I}^{\mathrm{f}} \end{bmatrix} = \begin{bmatrix} \mathbf{V}^{\mathrm{r}} \\ \mathbf{V}^{\mathrm{f}} \end{bmatrix}. \tag{4}$$

Upon multiplying both sides by $[\mathbf{Z}^{\mathrm{rr}}, \mathbf{0}; \mathbf{0}, \mathbf{Z}^{\mathrm{ff}}]^{-1}$, the final solution for the combined problem can be obtained as

$$\begin{bmatrix} \mathbf{I}^{\mathrm{r}} \\ \mathbf{I}^{\mathrm{f}} \end{bmatrix} = \left(\begin{bmatrix} \mathbf{1} & \mathbf{0} \\ \mathbf{0} & \mathbf{1} \end{bmatrix} + \begin{bmatrix} \mathbf{Z}^{\mathrm{rr}} & \mathbf{0} \\ \mathbf{0} & \mathbf{Z}^{\mathrm{ff}} \end{bmatrix}^{-1} \begin{bmatrix} \mathbf{0} & \mathbf{Z}^{\mathrm{rf}} \\ \mathbf{Z}^{\mathrm{fr}} & \mathbf{0} \end{bmatrix} \right)^{-1} \begin{bmatrix} \mathbf{I}^{\mathrm{r}}_0 \\ \mathbf{I}^{\mathrm{f}}_0 \end{bmatrix}. \tag{5}$$

where $\mathbf{1}$ is the identity matrix, and where the initial expansion coefficient vector for the reflector current $\mathbf{I}^{\mathrm{r}}_0 = (\mathbf{Z}^{\mathrm{rr}})^{-1}\mathbf{V}^{\mathrm{r}}$, while for the feed current $\mathbf{I}^{\mathrm{f}}_0 = (\mathbf{Z}^{\mathrm{ff}})^{-1}\mathbf{V}^{\mathrm{f}}$. These initial currents are obtained by solving the reflector and antenna feed problems in isolation. It is observed that Eq. (5) is of the form

$$\mathbf{I} = \left(\mathbf{1} + (\mathbf{Z}^{\mathrm{d}})^{-1}\mathbf{Z}^{\mathrm{o}}\right)^{-1} \mathbf{I}_0 \tag{6}$$

where

$$\mathbf{Z}^{\mathrm{d}} = \begin{bmatrix} \mathbf{Z}^{\mathrm{rr}} & \mathbf{0} \\ \mathbf{0} & \mathbf{Z}^{\mathrm{ff}} \end{bmatrix} \quad \text{and} \quad \mathbf{Z}^{\mathrm{o}} = \begin{bmatrix} \mathbf{0} & \mathbf{Z}^{\mathrm{rf}} \\ \mathbf{Z}^{\mathrm{fr}} & \mathbf{0} \end{bmatrix}. \tag{7}$$

Upon using the matrix equivalent of the scalar infinite geometric series $\sum_{n=0}^{\infty} r^n = (1-r)^{-1}$, where $|r| < 1$ for the series to converge, Eq. (6) can be rewritten in terms of the infinite series

$$\mathbf{I} = \sum_{n=0}^{\infty} \left(-(\mathbf{Z}^{\mathrm{d}})^{-1}\mathbf{Z}^{\mathrm{o}}\right)^n \mathbf{I}_0 \tag{8}$$

[1]Here $\mathbf{Z}^{\mathrm{ff}}$ includes the effect of the antenna port terminations [32].

where the spectral radius $\rho((\mathbf{Z}^{\mathrm{d}})^{-1}\mathbf{Z}^{\mathrm{o}}) \stackrel{\mathrm{def}}{=} \max_i(|\lambda_i|)$ of the matrix $(\mathbf{Z}^{\mathrm{d}})^{-1}\mathbf{Z}^{\mathrm{o}}$ with eigenvalues $\{\lambda_i\}$ must be smaller than unity for the series to converge. The physical multiscattering interpretation of the geometric series in (8) is apparent when expanding it as:

$$\mathbf{I} = \mathbf{I}_0 - (\mathbf{Z}^{\mathrm{d}})^{-1}\mathbf{Z}^{\mathrm{o}}\mathbf{I}_0 + \left((\mathbf{Z}^{\mathrm{d}})^{-1}\mathbf{Z}^{\mathrm{o}}\right)^2\mathbf{I}_0 + \ldots = \sum_{n=0}^{\infty}\mathbf{I}_n \quad (9)$$

where the last summation is supposed to add up successively smaller contributions for the currents on the reflector and antenna feed in order to converge. It is conjectured that $\rho((\mathbf{Z}^{\mathrm{d}})^{-1}\mathbf{Z}^{\mathrm{o}}) \ll 1$ for the practical reflector antenna systems that we consider, since most of the energy is radiated out after each iteration and where the feeds have relatively small aperture areas (weak reflector-feed coupling), so that the sum converges within a few iterations (*cf.* Sec. IV-A and IV-C). Finally, using (7), the infinite series summation in Eq. (9) can be written in the cross-coupled recursive scheme

Reflector	Feed
$\mathbf{I}^{\mathrm{r}} = \sum_{n=0}^{\infty}\mathbf{I}^{\mathrm{r}}_n$ (10a)	$\mathbf{I}^{\mathrm{f}} = \sum_{n=0}^{\infty}\mathbf{I}^{\mathrm{f}}_n$ (11a)
$\mathbf{I}^{\mathrm{r}}_{n+1} = -(\mathbf{Z}^{\mathrm{rr}})^{-1}\mathbf{Z}^{\mathrm{rf}}\mathbf{I}^{\mathrm{f}}_n$ (10b)	$\mathbf{I}^{\mathrm{f}}_{n+1} = -(\mathbf{Z}^{\mathrm{ff}})^{-1}\mathbf{Z}^{\mathrm{fr}}\mathbf{I}^{\mathrm{r}}_n$ (11b)
$\mathbf{I}^{\mathrm{r}}_0 = (\mathbf{Z}^{\mathrm{rr}})^{-1}\mathbf{V}^{\mathrm{r}}_0$ (10c)	$\mathbf{I}^{\mathrm{f}}_0 = (\mathbf{Z}^{\mathrm{ff}})^{-1}\mathbf{V}^{\mathrm{f}}_0$ (11c)

where $\mathbf{V}^{\mathrm{r}}_0 = \mathbf{V}^{\mathrm{r}}$ and $\mathbf{V}^{\mathrm{f}}_0 = \mathbf{V}^{\mathrm{f}}$ are the initial excitation voltage vectors of the reflector and the feed, respectively (in transmit situation $\mathbf{V}^{\mathrm{r}}_0 = \mathbf{0}$).

The cross-coupled recursive scheme as formulated by Eqs. (10) and (11) is exemplified in Fig. 2 as a five-step procedure, in which the problem is first solved in isolation to obtain $\mathbf{I}^{\mathrm{r}}_0$ and $\mathbf{I}^{\mathrm{f}}_0$. Afterwards, the feed current $\mathbf{I}^{\mathrm{f}}_0$ is used to induce the reflector current $\mathbf{I}^{\mathrm{r}}_1$, which is then added up to the initial reflector current. Likewise, the initial reflector current $\mathbf{I}^{\mathrm{r}}_0$ is used to induce the feed current $\mathbf{I}^{\mathrm{f}}_1$, which is then added to the initial feed current, and so forth. It is pointed out that this recursive scheme can be used for any pair of radiating and/or scattering objects, provided that the system is weakly coupled – due to radiation and/or dissipation losses – in order to obtain a convergent solution.

Rather than computing the reflector and feed currents through the large-size MoM matrix blocks $\mathbf{Z}^{\mathrm{rr}}$, $\mathbf{Z}^{\mathrm{rf}}$, $\mathbf{Z}^{\mathrm{fr}}$, and $\mathbf{Z}^{\mathrm{ff}}$, additional computational and memory efficient techniques can be used for the rapid computation of these currents at each iteration; we propose to employ the Physical Optics (PO) current on the reflector and invoke the Characteristic Basis Function Method (CBFM, [33]) as a MoM enhancement technique for computing the current on the feed.

Note that (11b) represents the MoM matrix solution $\mathbf{I}^{\mathrm{f}}_{n+1} = (\mathbf{Z}^{\mathrm{ff}})^{-1}\mathbf{V}^{\mathrm{f}}_n$, where $\mathbf{V}^{\mathrm{f}}_n = -\mathbf{Z}^{\mathrm{fr}}\mathbf{I}^{\mathrm{r}}_n$ is the voltage excitation vector of the feed at iteration n. Hence, one can obviate the construction of the large matrix $\mathbf{Z}^{\mathrm{fr}}$ by directly computing $\mathbf{V}^{\mathrm{f}}_n$. This is done through testing the incident electric field $\boldsymbol{E}^{\mathrm{i,f}}_n(\boldsymbol{r})$

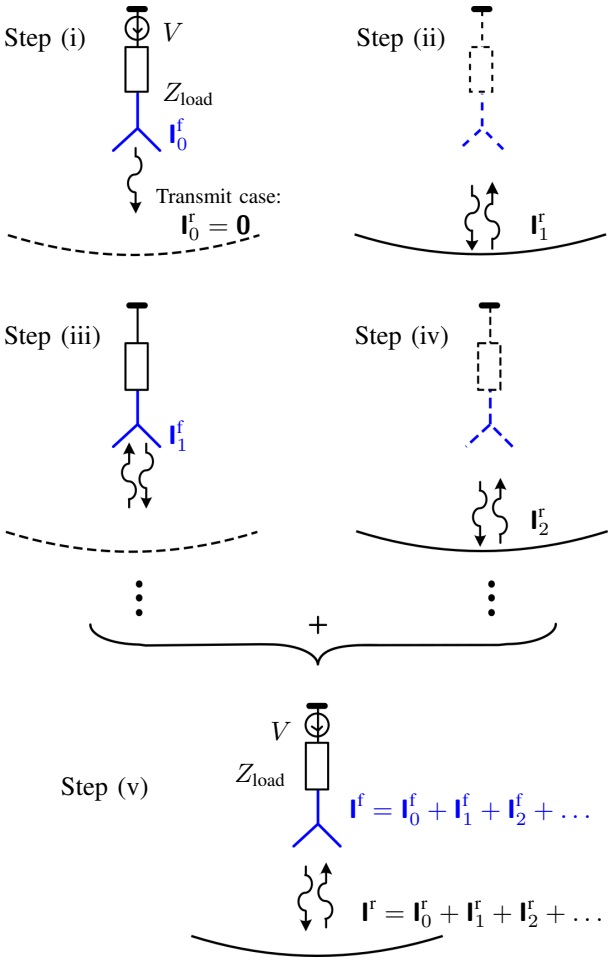

Fig. 2. Illustration of the cross-coupled iterative scheme for multiscattering analysis of the feed-reflector interaction effects, as formulated by Eqs. (10) and (11): (i) The antenna feed radiates in the absence of reflector; (ii) the radiated field from feed scatters from the reflector; (iii) the scattered reflector field is incident on the terminated feed and re-scatters; (iv) the re-scattered field from the feed is incident on the reflector; etc. (v) the final solution for the current is the sum of the induced currents.

by the P basis functions $\{\boldsymbol{f}^{\mathrm{f}}_p\}_{p=1}^{P}$ supported by the feed, i.e.,

$$\mathbf{I}^{\mathrm{f}}_{n+1} = -\left(\mathbf{Z}^{\mathrm{ff}}\right)^{-1}\left[\langle \boldsymbol{E}^{\mathrm{i,f}}_n, \boldsymbol{f}^{\mathrm{f}}_1\rangle, \langle \boldsymbol{E}^{\mathrm{i,f}}_n, \boldsymbol{f}^{\mathrm{f}}_2\rangle, \ldots, \langle \boldsymbol{E}^{\mathrm{i,f}}_n, \boldsymbol{f}^{\mathrm{f}}_P\rangle\right]^T \quad (12)$$

where $\boldsymbol{E}^{\mathrm{i,f}}_n$ is taken equal to the E-field radiated by the PO current $\mathbf{J}^{\mathrm{r}}_n$ on the reflector, which is directly known through the reflector incident H-field $\mathbf{H}^{\mathrm{i,r}}_n$, so that there is no need to compute the basis function coefficients $\mathbf{I}^{\mathrm{r}}_n$ explicitly.

For electrically small triangular cells on the reflector surface (with edge length $< 0.2\lambda$), the smoothly-varying PO current can be considered constant over each cell, so that the electric field produced by the qth reflector triangle at the pth observation point, $\boldsymbol{E}^{\mathrm{i,f}}_{n,pq}$, can be computed through the near-field formula for an incremental electric current source, i.e. [34, p. 102],

$$\boldsymbol{E}^{\mathrm{i,f}}_{n,pq} = \frac{-j\eta k}{4\pi}\left[C_{1;pq}\boldsymbol{\ell}_{n,q} - C_{2;pq}(\boldsymbol{\ell}_{n,q}\cdot\hat{\boldsymbol{r}}_{pq})\hat{\boldsymbol{r}}_{pq}\right]\frac{e^{-jkr_{pq}}}{r_{pq}} \quad (13)$$

where

$$C_{1;pq} = 1 + \frac{1}{jkr_{pq}} - \frac{1}{(kr_{pq})^2}, \quad C_{2;pq} = 3C_{1;pq} - 2, \quad (14)$$

and where the dipole moment is computed as $\boldsymbol{\ell}_{n,q} = \boldsymbol{J}^{\mathrm{r}}_{n,q} A_q$, with A_q the area of qth reflector triangle ($q = 1, 2, \ldots, Q$). Hence, by using the expression for the PO current for $\boldsymbol{J}^{\mathrm{r}}_{n,q}$ [35, p. 343], we find that

$$\boldsymbol{\ell}_{n,q} = 2A_q \hat{\boldsymbol{n}}_q \times \boldsymbol{H}^{\mathrm{i,r}}_n(\boldsymbol{r}^{\mathrm{r}}_q), \quad (15)$$

where $\boldsymbol{r}^{\mathrm{r}}_q \in S$ is the centroid of the qth triangle on the reflector surface S (*cf.* Fig. 3); $\hat{\boldsymbol{n}}_q$ is the normal to the reflector surface of the qth triangle, and $\boldsymbol{H}^{\mathrm{i,r}}_n$ is the incident H-field generated by the feed current at iteration n. Using (15) and (13), the incident E-field in (12) is readily computed as $\boldsymbol{E}^{\mathrm{i,f}}_{n,p} = \sum_{q=1}^{Q} \boldsymbol{E}^{\mathrm{i,f}}_{n,pq}$. The computation of (11b) can be further accelerated as explained in Sec. III-A.

Once $\mathbf{V}^{\mathrm{f}}_n$ is known, the current on the feed $\mathbf{I}^{\mathrm{f}}_{n+1}$ at the next iteration can be computed through solving the linear system of equations $\mathbf{Z}^{\mathrm{ff}}\mathbf{I}^{\mathrm{f}}_{n+1} = \mathbf{V}^{\mathrm{f}}_n$. For complex-shaped and electrically large antennas, such as the wideband tapered slot antenna array feeds [13], it becomes necessary to use both memory- and time-efficient methods, such as the CBFM. The CBFM solves the current $\mathbf{I}^{\mathrm{f}}_{n+1}$ through the following set of equations:

$$\begin{cases} \mathbf{I}^{\mathrm{f}}_{n+1} & = \mathbf{J}^{\mathrm{CBF}}\mathbf{I}^{\mathrm{CBF}}_{n+1} \\ \mathbf{I}^{\mathrm{CBF}}_{n+1} & = \mathbf{Z}^{\mathrm{CBF}}\mathbf{V}^{\mathrm{CBF}}_{n} \\ \mathbf{V}^{\mathrm{CBF}}_{n} & = (\mathbf{J}^{\mathrm{CBF}})^T\mathbf{V}^{\mathrm{f}}_{n} \end{cases}, \quad (16)$$

where $\mathbf{Z}^{\mathrm{CBF}} = (\mathbf{J}^{\mathrm{CBF}})^T\mathbf{Z}^{\mathrm{ff}}\mathbf{J}^{\mathrm{CBF}}$ is the CBFM-reduced MoM matrix of the feed; $\mathbf{J}^{\mathrm{CBF}} = [\mathbf{J}^{\mathrm{CBF}}_1|\mathbf{J}^{\mathrm{CBF}}_2|\ldots|\mathbf{J}^{\mathrm{CBF}}_L]$ is the column-augmented matrix of Characteristic Basis Functions (CBFs), i.e., $\mathbf{J}^{\mathrm{CBF}}_l$ is the set of CBFs (pre-defined expansion coefficient vectors) on the lth macro domain of the feed, and $l = 1 \ldots L$, where L is number of macro domains on the feed. Specific details on the generation of CBFs can be found in [33], where the feed is analyzed as a phased array antenna in the absence of the reflector. Also, it is worth pointing out that the computation of $\mathbf{Z}^{\mathrm{CBF}}$ (i.e. the CBF coupling terms) is performed in a time-efficient manner through utilizing the Adaptive Cross Approximation (ACA) algorithm [36].

III. Acceleration of the Field Computations

The above-described iterative CBFM-PO approach requires the field to be computed at numerous points on both the feed and the reflector surfaces, thereby rendering the field computations inefficient, in particular for complex-shaped electrically large feed antennas employing hundreds of thousands of low-level basis functions. Similarly, one has to cope with a computational burden when calculating the PO equivalent current on electrically large reflectors.

However, it has been shown that the PO radiated field for on-axis beams can be approximated rather accurately through a single plane wave (PW) field [10], [37]. This observation opts for employing a Plane Wave Spectrum (PWS) to speed up the field computations [38]–[40]. In fact, the on-axis PW corresponds to the Geometrical Optics (GO) contribution of the PO-radiated field (originating from the stationary phase point), as will be demonstrated in Sec. III-A, while the higher-order PWs are needed to model the edge-diffracted fields from the rim of the reflector, which are associated with the end-point contributions of the PO current in the radiation integral.

Furthermore, one can accelerate the computation of the PO current itself by using an interpolation technique of the near-field antenna feed pattern as detailed below.

A. Plane Wave Spectrum Expansion – FFT

With reference to Fig. 3, a grid of sampling points in the xy-plane P in front of the feed at $z = 0$ is chosen for the expansion of the PO radiated field in terms of a PWS. Each PW propagates to a specific observation point $\boldsymbol{r}$ on the feed where the field $\boldsymbol{E}^{\mathrm{i,f}}$ is tested. This process of field expansion and PW propagation is realized through the application of the truncated Fourier Transform pair [38]

$$\boldsymbol{A}(k_x, k_y) = \frac{1}{2\pi} \int_{-y_{\max}}^{y_{\max}} \int_{-x_{\max}}^{x_{\max}} \boldsymbol{E}^{\mathrm{i,f}}(x, y, z = 0) e^{j(k_x x + k_y y)} \, \mathrm{d}x \, \mathrm{d}y \quad (17a)$$

$$\boldsymbol{E}^{\mathrm{i,f}}(\boldsymbol{r}) = \frac{1}{2\pi} \int_{-k_x^{\max}}^{k_x^{\max}} \int_{-k_y^{\max}}^{k_y^{\max}} \boldsymbol{A}(k_x, k_y) e^{-jk_z z} e^{-j(k_x x + k_y y)} \, \mathrm{d}k_x \, \mathrm{d}k_y \quad (17b)$$

where

$$k_z = \begin{cases} \sqrt{k^2 - k_x^2 - k_y^2} & \text{if } k^2 > k_x^2 - k_y^2 \\ -j\sqrt{k_x^2 - k_y^2 - k^2} & \text{otherwise.} \end{cases}, \quad (18)$$

and where the spectrum of PWs is limited to only those that are incident on the feed from directions within an angle subtended by the reflector and seen from the center of the plane P (see Fig. 3); hence, the maximum wavenumbers $k_x^{\max}$ and $k_y^{\max}$

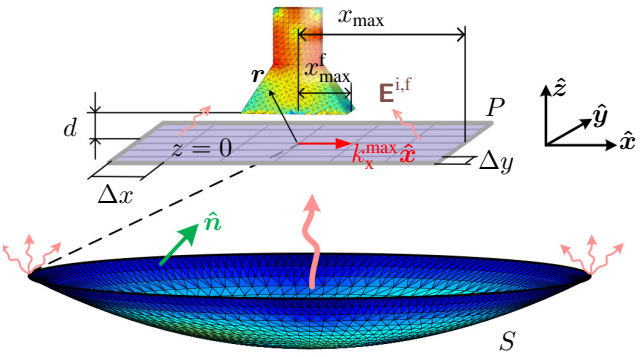

Fig. 3. The FFT-enhanced PWS expansion method for the fast computation of the feed current due to the E-field from the reflector. Firstly, the incident field $\boldsymbol{E}^{\mathrm{i,f}}$ is sampled in the xy plane P in front of the feed in order to obtain the sampled PWS $\boldsymbol{A}(k_x, k_y)$; Secondly, each spectral PW propagates to an observation point $\boldsymbol{r}$ on the feed where $\boldsymbol{E}^{\mathrm{i,f}}$ is tested to compute the induced feed current.

in (17b) are chosen to be equal to

$$k_x^{\max} = k_y^{\max} = k \sin\left[\tan^{-1}\left(\frac{8\left(\frac{F}{D}\right)}{16\left(\frac{F}{D}\right)^2\left[1-\left(\frac{F}{d}\right)^{-1}\right]-1}\right)\right] \tag{19}$$

where $k = 2\pi/\lambda$ is the free-space wavenumber; F and D are the focal distance and diameter of the parabolic reflector, respectively; and d is the distance between the plane P and the geometrical focal plane of the reflector. Since the maximum spectral components $k_x^{\max}$ and $k_y^{\max}$ are known, the minimum step size Δx and Δy for the spatial sampling of the field is found from Nyquist's sampling theorem:

$$\Delta x = \pi/k_x^{\max}, \qquad \Delta y = \pi/k_y^{\max}. \tag{20}$$

Furthermore, if (17) is evaluated through a Fast Fourier Transform (FFT), the discretely sampled field functions are periodic in both the spatial and frequency domains. To minimize the field artifacts that are associated with this periodicity, $x_{\max}$ and $y_{\max}$ must be chosen sufficiently large, that is, at least equal to the maximum size $x_{\max}^{\mathrm{f}}$ and $y_{\max}^{\mathrm{f}}$ of the feed coordinates. The examination of how the error of the feed current depends on $x_{\max}$ and $y_{\max}$ is presented in Sec. IV-B.

As a result, the total number of sampling points in the x and y directions are $N_x = 2x_{\max}/\Delta x$ and $N_y = 2y_{\max}/\Delta y$, respectively, and the spectral spacings and the spatial extents are related through $\Delta k_x = 2k_x^{\max}/N_x = \pi/x_{\max}$ and $\Delta k_y = 2k_y^{\max}/N_y = \pi/y_{\max}$.

B. Near-Field Interpolation

While the previous section describes how the PWS-expanded E-field from the reflector accelerates the computation of the induced feed current, this section explains how the reflector incident H-field can be computed for the rapid determination of the induced PO current. For this purpose, the radiated H-field from the feed is first computed at a coarse grid on the reflector surface (white circles in Fig. 4), after which the field at each triangle is determined on the reflector (yellow square markers) through an interpolation technique. This interpolation technique de-embeds the initially sampled field to a reference sphere with radius R whose origin coincides with the phase center of the feed to assure that the phase of the de-embedded field will be slowly varying. Consequently, relatively few sampling points are required for the field interpolation, after which the interpolated fields are propagated back to the reflector.

In summary, and with reference to Fig. 4, the H-field interpolation algorithm for determining the reflector PO current

1) Defines a grid on the reflector surface (white circles) for computing the H-field.
2) De-embeds the H-field to a reference sphere around the feed phase center (green points):

$$\boldsymbol{H}_m^{\mathrm{sph}} = \boldsymbol{H}_m d_m e^{jkd_m}, \tag{21}$$

where d_m is the distance between the reflector surface and the sphere of radius R along the line connecting the mth sample point on the reflector and the feed phase center.
3) Computes the fields on the sphere in the same directions as the reflector triangle centroids are observed (blue square markers) through interpolating the fields at the adjacent (green) points.
4) Propagates the field to the reflector surface; that is, at the qth triangle, the H-field

$$\boldsymbol{H}^{\mathrm{i,r}}(\boldsymbol{r}_q^{\mathrm{r}}) = \boldsymbol{H}_q^{\mathrm{sph}} d_q^{-1} e^{-jkd_q}. \tag{22}$$

5) Computes the reflector PO current by using (15).

Sec. IV-B examines the error in the reflector current as a function of the sample grid density, in addition to the improvement in computation time that this method offers.

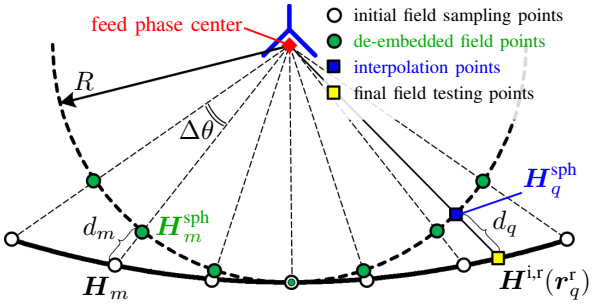

Fig. 4. The near-field interpolation technique for the rapid determination of the induced PO current on the reflector.

IV. Numerical Results

In this section, we start with the validation of the proposed iterative MoM-PO approach for a relatively strongly coupled feed-reflector system, comprised of a small reflector ($D = 14\lambda$) fed by a dipole antenna over a ground plane for which we examine the convergence rate of the solution for the antenna input impedance. Furthermore, we validate the frequency-dependent radiation characteristics of a dipole array feed through the commercially available software FEKO [41]. Afterwards, a relative error analysis of the antenna transmit

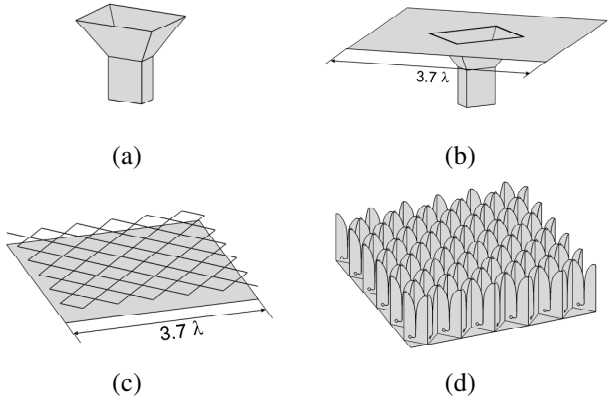

Fig. 5. Considered feed geometries (in addition to the dipole feed with PEC ground plane): (a) a classical pyramidal horn with aperture length $\sim 1\lambda$; (b) the same horn but with extended ground plane ($\sim 3.7\lambda$), where the ground plane may model the presence of a large feed cabin; (c) an antenna array consisting of 121 0.45λ-dipoles above a ground plane of the same size; (d) the same array, but with the dipoles replaced by wideband tapered slot Vivaldi antennas.

characteristics is performed when the acceleration techniques in Sec. III are utilized. Finally, a more practical study is carried out, where the impact of the feed-reflector coupling on the performance of the antenna reflector system for different types of low- and high-scattering feeds is analyzed and discussed. For the latter study, two parabolic reflectors with diameters $D = 38\lambda$ and 118λ are considered, in conjunction with the four types of feeds that are shown in Fig. 5. It is shown that the measured and simulated results for a 121-element Vivaldi PAF, which is installed on the Westerbork Synthesis Radio Telescope, are in very good agreement.

The MoM computations have been carried out on a 64-bit openSUSE Linux server (kernel version: 2.6.37.6-0.20-desktop), equipped with 144 GB of RAM and two quad-core Intel(R) Xeon(R) E5640 CPUs, each operating at 2.67 GHz. The FEKO Suite 6.0 EM solver runs on an Ubuntu Linux server (kernel-release: 2.6.32-21-server), equipped with a Dual Core AMD Opteron Processor 275 at 2.2 GHz with 16 GB of RAM.

A. Validation of the Iterative Approach

For validating the implemented iterative MoM-PO approach, a relatively small reflector ($D = 14\lambda$, $F/D = 0.35$) fed by a 0.5λ-dipole spaced 0.25λ above an $1\lambda \times 1\lambda$ and a $2\lambda \times 2\lambda$ PEC ground plane has been simulated, both by the proposed iterative and plain MoM approach. The dipole reflection coefficient as a function of the iteration count is shown in Fig. 6(a). Even though the feed-reflector coupling is relatively large due to a relatively large blockage area of the high-scattering feed, convergence of the impedance down to 0.1% relative error level, measured as a change between the last two iterations, is seen to occur within 5 and 9 iterations for the $1\lambda \times 1\lambda$ and $2\lambda \times 2\lambda$ PEC ground planes, respectively. This error ϵ_n at iteration n is computed as

$$\epsilon_n = \left(\sqrt{\sum_i |I_i^n - I_i^{n-1}|^2} \Big/ \sqrt{\sum_i |I_i^n|^2} \right) \times 100\%. \quad (23)$$

The small residual error of order 1% is a result of the PO-approximated reflector current. Fig. 6(b) shows how the

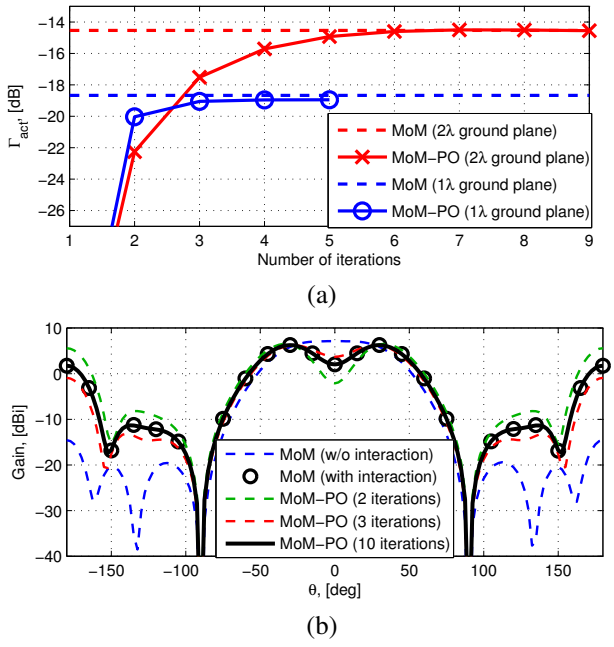

(a)

(b)

Fig. 6. The convergence of the feed radiation characteristics in the presence of the reflector as a function of the number of Jacobi iterations, in terms of: (a) the dipole input reflection coefficient, and; (b) the dipole illumination pattern at 1 GHz (ground plane size is $2\lambda \times 2\lambda$). The convergence as a function of the dipole load impedance is analyzed for a dipole antenna array feeding a 38λ reflector.

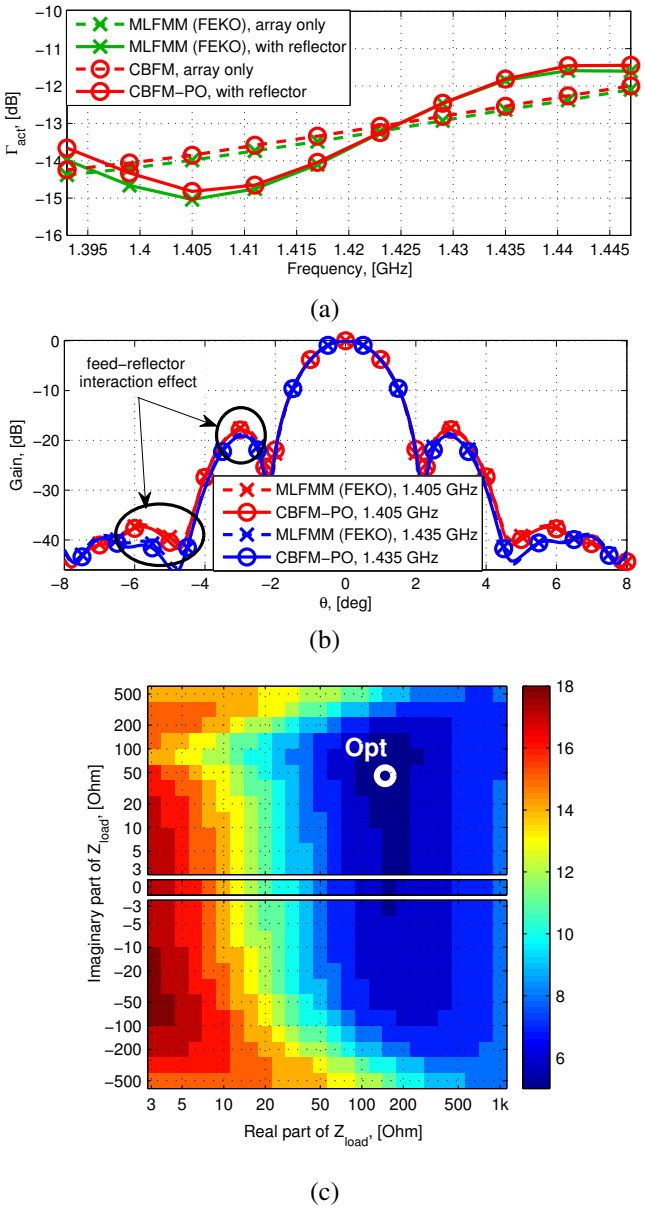

(a)

(b)

(c)

Fig. 7. (a) The magnitude of the active reflection coefficient of the most excited antenna array dipole element feeding a 38λ reflector as a function of frequency, and; (b) reflector antenna radiation pattern, simulated in FEKO (MLFMM) and using the described iterative CBFM-PO approach; (c) the number of required iterations for reaching convergence (error in feed current less than 0.5%). Interesting fact: the round marker indicates the impedance that maximizes the decoupling efficiency (=power-matched case) when the array feed is used as a broadside-scanned aperture array, which also happens to coincide with the minimum number of iterations (=low multiscattering effect).

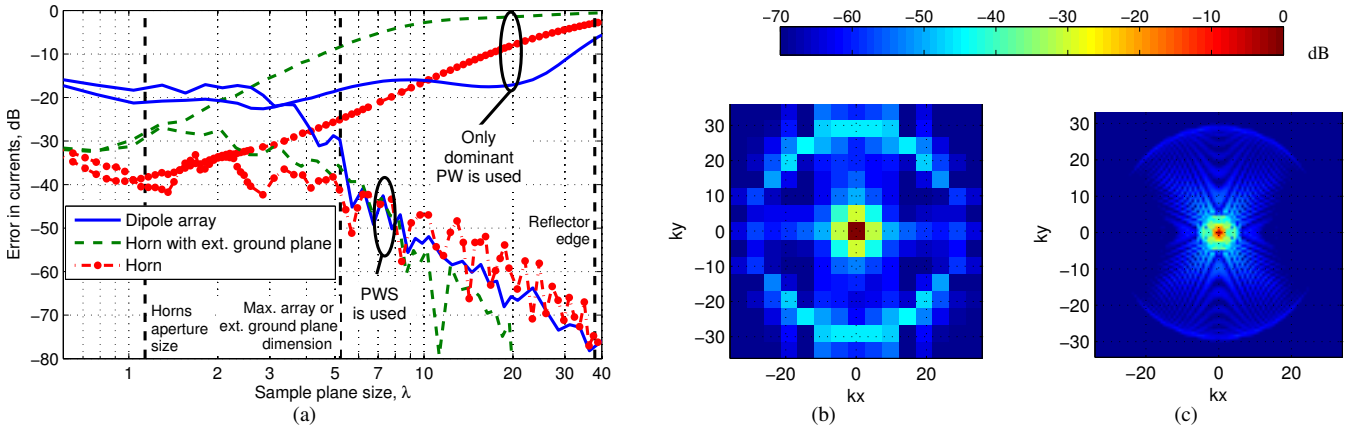

Fig. 8. (a) The relative error in induced feed currents [*cf.* (24)] as a function of the FFT sampling plane size P; (b) the magnitude of the spatial frequency spectrum $|A_{\rm co}(k_x, k_y)|$ (i.e. plane wave spectrum) for the 38λ reflector fed by the dipole array in case the FFT grid size is equal to size of the feed, and (c) when it is eight times the feed size.

forward gain of the dipole illumination pattern changes due to the feed-reflector coupling as the number of iterations increases.

For cross-code validation purposes, a larger and more complex 38λ reflector ($F/D = 0.35$) fed by an 121-dipole array feed has been analyzed [*cf.* Fig. 5(c)], both by the proposed iterative approach and the commercial FEKO software. Fig. 7(a,b) demonstrates a good agreement between the reflector antenna radiation patterns (includes the feed blockage effect) and the magnitudes of the computed active reflection coefficients as a function of frequency, where the frequency interval Δf of the oscillation period is consistent with the electrical distance between the feed and the reflector vertex, i.e., $\Delta f = c/2F$. Here, the optimal port termination that maximizes the array decoupling efficiency [8] was found through Matlab's "fminsearch" unconstrained nonlinear optimization routine (Nelder-Mead simplex direct search method) and was found to be $147 + 45.6j\ \Omega$. Thus far, practical PAF antenna elements have been optimized in phased array mode, broadside scan, using periodic boundary conditions in EM simulation software [42], hence, here too, the co-polarized elements of the array feed are excited in-phase to determine the optimal port loading. This optimal impedance is marked on Fig. 7(c) (and Fig. 11), where its plot shows the number of iterations – required to obtain an error in the dipole array feed current between the two last iterations less than 0.5% – as a function of the array loading. Note the interesting fact that the minimum number of iterations (=lowest multiscattering effect) occurs when the array is optimally loaded (=power matched), which is in accordance with our expectations, and this applies even though the antenna load impedance has been found for the aperture-array-excited case.

B. Field Approximation Errors

Sec. III-A and III-B describe a field expansion and interpolation technique for accelerating the feed-reflector interaction computations, respectively. In this section, we analyze the reflector induced feed current when the field from the reflector is expanded in terms of a truncated spectrum of plane waves, and compute the error in the feed current relative to a direct "full-wave" solution where the number of field modes radiated by the reflector equals the number of reflector triangles (=number of incremental dipole sources on the reflector). The distance d between the feed and the sampling plane P (*cf.* Fig. 3) has been chosen equal to 0.5λ in all PWS computations; in fact, our study shows that the selection of d in the range of $0.1 \ldots 5\lambda$ has a negligible ($< 0.7\%$) effect on the antenna characteristics, such as the aperture efficiency, even when the size of the plane P is kept the same. Both the relative error of the feed induced PO-reflector current and how the near-field interpolation grid density affects this error will be analyzed afterwards. Furthermore, the errors in the feed and reflector currents, as well as those in the gain of the antenna reflector system and the input impedance of the feed, will be summarized in a table.

The relative error between vector (or matrix) quantities – such as between the current expansion coefficient vectors $\mathbf{I}^{\rm approx}$ and $\mathbf{I}^{\rm ref}$ for the iterative CBFM-PO solution with and without field approximations, respectively – is computed as

$$\epsilon_1 = \left(\sqrt{\sum_i |I_i^{\rm ref} - I_i^{\rm approx}|^2} \Big/ \sqrt{\sum_i |I_i^{\rm ref}|^2} \right) \times 100\%, \quad (24)$$

while the relative error for scalar functions (antenna gain, impedance characteristics, etc.), is computed as

$$\epsilon_2 = \left(|A^{\rm ref} - A^{\rm approx}| / |A^{\rm ref}| \right) \times 100\%. \quad (25)$$

Fig. 8(a) illustrates the relative error in the feed surface current as a function of the FFT sampling plane size when the PWS is employed for expanding the reflector radiated field (for PWS parameters see Sec. III-A), and when only the dominant on-axis PW term is used. As expected, the error decreases for an increasing sampling plane size, since more spectral PW terms are taken into account while the effect of the FFT-related periodic continuation of the spatial aperture field decreases. Henceforth, we choose the sampling plane size equal to that of the feed, for which the feed current error is about -35 dB for all the considered feeds, while it represents a good compromise from both a minimum number of sampling

TABLE I
ERRORS DUE TO APPLYING THE FIELD APPROXIMATIONS, %

	Feed surface current		Reflector surface current		Gain (on-axis)		Gain (@−3 dB)		Impedance	
Reflector diameter D	**38λ**	**118λ**	**38λ**	**118λ**	**38λ**	**118λ**	**38λ**	**118λ**	**38λ**	**118λ**
Feed: Pyramidal horn										
PWS approximation	0.09	0.02	0.11	0.03	0.09	0.03	0.07	0.02	0.16	0.04
NFI approximation	0.01	<0.01	0.06	0.06	0.05	0.04	0.01	0.02	0.01	<0.01
Both approximations	0.09	0.02	0.13	0.07	0.13	0.07	0.07	0.04	0.15	0.04
Feed: Pyramidal horn with extended ground plane										
PWS approximation	0.28	0.02	0.41	0.02	0.06	0.01	0.09	0.01	0.44	0.04
NFI approximation	0.3	0.01	1.01	0.16	0.16	0.07	0.37	0.07	0.52	0.02
Both approximations	0.53	0.03	1.02	0.16	0.15	0.08	0.34	0.07	0.88	0.05
Feed: 121-element dual-polarized dipole array										
PWS approximation	0.05	0.02	0.1	0.02	0.03	0.01	0.01	0.01	0.03	0.01
NFI approximation	0.02	0.01	0.21	0.20	0.09	0.07	0.12	0.13	0.02	0.01
Both approximations	0.06	0.02	0.23	0.21	0.10	0.07	0.13	0.14	0.05	0.02

TABLE II
TOTAL SIMULATION TIME (FOR $D = 118\lambda$ REFLECTOR)

	Horn	Horn with ground plane	Dipole array	Vivaldi array
MoM-PO, no approximations	70 min (100%)	192 min (100%)	801 min (100%)	3906 min (100%)
PWS approximation	27 min (39.0%)	63 min (32.9%)	190 min (23.8%)	1312 min (33.6%)
NFI approximation	57 min (81.3%)	152 min (79.4%)	548 min (68.5%)	2108 min (54.0%)
Both approximations	13 min (19.2%)	17 min (9.0%)	16 min (2.0%)	33 min (0.9%)

points and accuracy point of view. Conversely, if only the dominant on-axis PW term is used to approximate the reflector field, the error increases when the plane P becomes larger. This is due to the tapering of the reflector scattered field which becomes more pronounced when the plane size P increases, so that the PW amplitude $A(k_x, k_y)$ is underestimated when using the field averaging in (17a) for $k_x = k_y = 0$, as opposed to the direct on-axis point sampling method that has been presented in [10].

Note that the magnitude of the co-polarized spatial frequency spectrum $|A_{\text{co}}(k_x, k_y)|$ in Figs. 8(b) and (c) exhibit several interesting features; as expected, the dominant spectral component corresponds to the on-axis PW, for which $k_x = k_y = 0$, while the second strongest set of PWs originate from the rim of the reflector, as observed by the spectral ring structure for which $k_x^2 + k_y^2 = (k_x^{\max})^2 = (k_y^{\max})^2$.

Regarding the interpolation method for the radiated near-fields of the feed (Sec. III-B), Figs. 9(a) and (b) show that the error in the resulting induced reflector current depends on the angular step size $\Delta\theta$ and $\Delta\phi$ of the initial field sampling grid (before interpolation). As expected, the error increases when the sampling grid coarsens. Furthermore, the error is larger for larger feeds, especially for high-scattering ones, for which the scattered fields (i.e. 2nd iteration and further) vary more rapidly than for smaller low-scattering antennas for which a coarser grid can be applied.

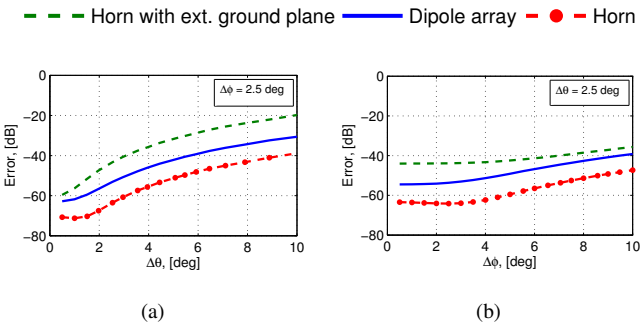

(a) (b)

Fig. 9. The interpolation error in the 38λ reflector current as a function of (a) the sampling step $\Delta\theta$, and (b) the sampling step $\Delta\phi$ of the near fields of the feed.

Table I summarizes the relative errors in both the currents and relevant antenna characteristics, while Table II shows how the simulation time of a "plain" iterative CBFM-PO (or MoM-PO) approach reduces when the field approximations of Sec. II are used. Note that the PWS approximation leads to a small relative error in the surface current of the high-scattering feed for the 38λ reflector, i.e. 0.28%, while if only a single on-axis PW is used, the relative error is found to be two orders larger [37]. It is also observed that, when applying the field approximations for both the reflector and feed, the error in the considered antenna characteristics remains less than 1%, while the computational speed advantage is significant, i.e., a factor 5 to 100, depending on the reflector size and feed complexity.

C. Feed-Reflector Antenna System Performance Study

The performance of several reflectors fed by low- and high-scattering feeds is studied in detail in this section. It is shown how the frequency ripple in the antenna radiation characteristics is formed and how the feed termination affects the magnitude of this ripple. The system performance and pros and cons of the different feeds are summarized in a table and discussed from a multiscattering point of view.

Fig. 10 illustrates the level of the total (including feed-reflector interaction) and the scattered field distributions in the aperture of a 38λ reflector fed by the horn with an extended

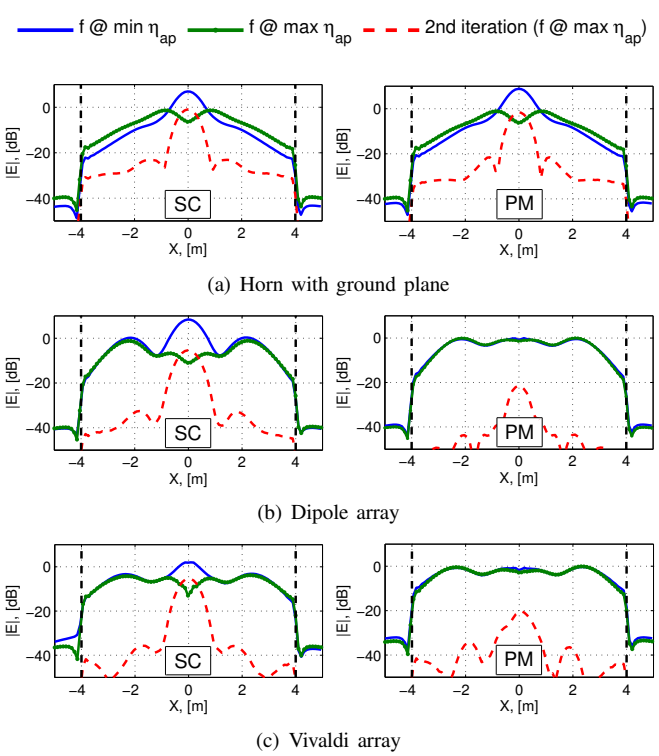

(a) Horn with ground plane

(b) Dipole array

(c) Vivaldi array

Fig. 10. Distribution of the field in the aperture of a 38λ reflector fed by: (a) horn with extended ground plane; (b) dipole array, and; (c) Vivaldi array. Left and right columns correspond to the short-circuited (SC) and average power-matched (PM) feeds, respectively.

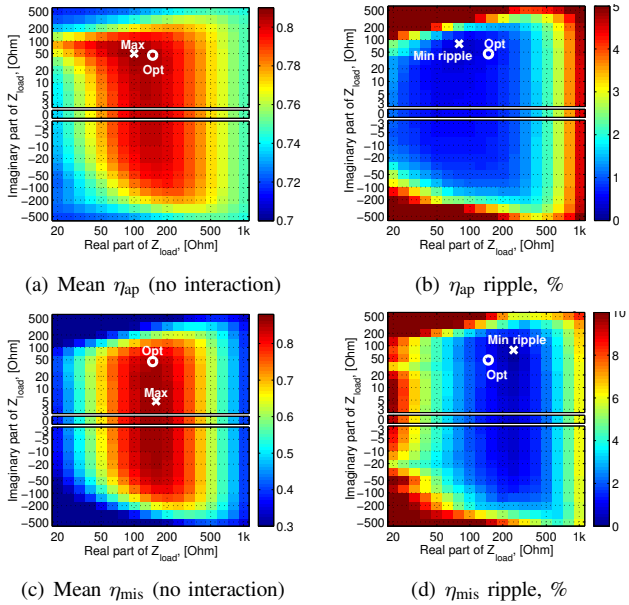

(a) Mean η_{ap} (no interaction)

(b) η_{ap} ripple, %

(c) Mean η_{mis} (no interaction)

(d) η_{mis} ripple, %

Fig. 11. Effect of the antenna port loading on (a) the aperture efficiency without feed-reflector coupling, and (b) aperture efficiency ripple when the feed-reflector coupling is present; (c),(d) the same for the mismatch efficiency. A 38λ reflector is fed by the 121-element dipole array. The round marker denotes the optimal load impedance that maximizes the decoupling efficiency (*cf.* Sec. IV-A).

ground plane, the dipole array, and the Vivaldi array, for both the short-circuited (left column) and the power-matched (right column) loading schemes. Although the short-circuited case is not very practical, it does showcase how two very different loading scenarios affect the aperture field variation, and how it depends on the type of the feed. The two solid lines in each sub-figure show the extrema that the aperture field distribution attains within one period of the ripple's frequency interval $\Delta f = c/2F$. The dashed lines show the aperture field due to the scattered field of the feeds. Clearly, for array feeds, the aperture field distribution is strongly dependent on the antenna port termination; the re-scattered fields from the array feeds affect the aperture field distribution significantly when the antenna ports are short-circuited, as opposed to the power-matched array feeds, whose scattered fields are significantly weaker. Note the differences in results for the horn with extended ground plane, for which the dominant part of the scattered field is primarily attributed to the metallic ground plane, while the impedance mismatch of the horn itself has only a minor effect (i.e. the residual component of the Radar Cross Section is large, but the antenna component is small [19]).

From the above analysis, one concludes that more Jacobi iterations are required to reach convergence for feeds that are poorly impedance matched as they tend to scatter a larger portion of the incident field (stronger multiscattering effects). It is therefore likely that the number of Jacobi iterations is closely related to the magnitude of the ripple on the antenna radiation characteristics; this fact is demonstrated in Fig. 11, which shows the aperture efficiency, mismatch factor [8], [43] and their ripples as a function of the port termination impedance. The ripple R_ν for a frequency-dependent parameter $\nu(f)$ is herein defined as

$$R_\nu = \frac{\max_f\left[\Delta\nu(f)\right] - \min_f\left[\Delta\nu(f)\right]}{\text{mean}_f\left[\nu_{\text{with\_coup}}(f)\right]} \times 100\%, \qquad (26)$$

where $\Delta\nu(f) = \nu_{\text{with\_coup}}(f) - \nu_{\text{no\_coup}}(f)$ is the difference between the considered parameter ν, with and without accounting for the feed-reflector coupling. The considered frequency band is herein taken relatively narrow as it corresponds to one period of the ripple only, i.e., $\Delta f = c/2F$. We further point out that these results apply to a feed that is excited at all its ports such as to realize a maximum gain pattern of the combined feed-reflector system, hereafter referred to as the Conjugate Field Match (CFM) beamformer. Furthermore, to be able to compare the results with the commonly employed uniformly excited array case analyzed above, the CFM excitations are fixed and determined only once for the optimal antenna port loading, i.e., pertaining to the uniformly excited array.

One concludes from Fig. 11(a) that the aperture efficiency is a function of the antenna port loading, and that the impedance for which η_{ap} attains a maximum is close to the optimal power-match impedance found in Sec. IV-A for the uniformly excited array case. This apparently even holds in the absence of the feed-reflector interactions, in which case the array illumination pattern has changed slightly due to perturbed array embedded element patterns while the CFM excitation coefficients remain unaltered. In Sec. IV-A we maximized the decoupling efficiency to find the optimal port loading. For the present CFM all-excited array case the decoupling efficiency reduces to the

TABLE III
MAXIMUM PARAMETER DIFFERENCE DUE TO FEED-REFLECTOR COUPLING EFFECT W.R.T. THE CASES WHEN NO COUPLING IS TAKEN IN ACCOUNT, %

	Feed surface current		Reflector surface current		Gain (on-axis)		Gain (@-3 dB)		Impedance	
Reflector diameter D	**38λ**	**118λ**	**38λ**	**118λ**	**38λ**	**118λ**	**38λ**	**118λ**	**38λ**	**118λ**
Pyramidal horn	7.9	2.5	4.2	1.3	2.0	0.6	4.0	2.2	15.1	4.7
Horn with ext. ground plane	23.2	3.5	65.1	11.9	19.2	3.4	29.4	3.6	43.4	6.1
Dipole array	13.8	4.2	3.2	0.8	1.8	0.3	3.7	0.7	5.8	1.7
Vivaldi array	14.1	4.1	3.4	1.0	1.9	0.3	3.4	0.4	4.6	1.4

TABLE IV
SYSTEM CHARACTERISTICS (AND THEIR RIPPLE) OVER FREQUENCY BAND

	38λ reflector				**118λ reflector**			
	Horn	**Horn + gnd**	**Dipole array**	**Vivaldi array**	**Horn**	**Horn + gnd**	**Dipole array**	**Vivaldi array**
η_{ill}	0.71 (7.2%)	0.67 (34.1%)	0.86 (1.0%)	0.92 (0.6%)	0.71 (2.2%)	0.72 (4.1%)	0.85 (0.4%)	0.92 (0.2%)
η_{mis}	0.992 (1.0%)	0.987 (5.1%)	0.830 (1.2%)	0.910 (0.9%)	0.999 (0.2%)	0.999 (0.2%)	0.853 (0.5%)	0.926 (0.4%)
T_{sp}	7.7 K (18%)	6.8 K (39%)	4.2 K (16.8%)	8.8 K (9.6%)	7.7 K (6.0%)	7.2 K (6.8%)	3.8 K (5.7%)	8.7 K (3.4%)

mismatch factor η_{mis}. The maximum of η_{mis} does, however, not coincide with the earlier optimal load impedance primarily due to the difference in array excitation schemes. Nonetheless, the observed quantities are only weakly dependent on impedance variations around their maximums. As for the feed-reflector-induced ripple of η_{ap} and η_{mis} [Fig. 11(b) and Fig. 11(d)], we can conclude that the η_{mis} ripple is more sensitive to variations in the array loading relative to the ripple in η_{ap}. In practice, however, when the amplifier/LNA impedance changes up to 10-20%, this only weakly affect η_{ap} and η_{mis} and their ripple.

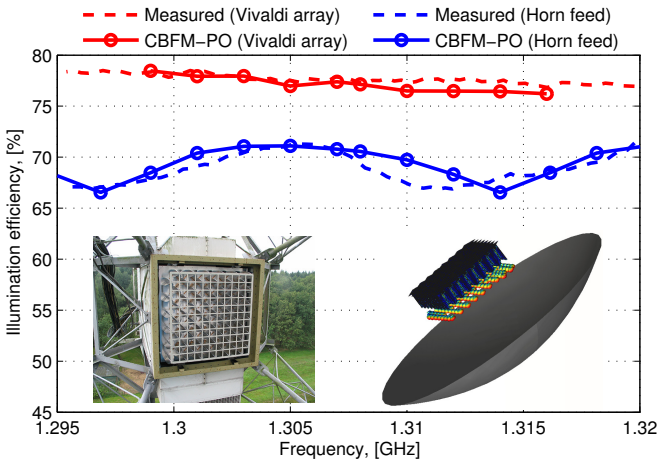

Fig. 12. Illumination efficiencies of the 118λ reflector antenna, either fed by the 121 Vivaldi PAF, or the single-horn feed. The CBFM-PO simulated results are compared to the measured ones for a 25 m reflector antenna of the Westerbork Synthesis Radio Telescope [4]. Bottom of the figure: a photo of the experimental PAF system placed at the focal region of the reflector, and an image of a smaller-scale PAF-reflector model.

Table III and IV summarize the maximum difference in mean values and ripple, respectively, of several other relevant antenna radiation characteristics when the feed-reflector coupling is taken into account. For the computation of this difference Eq. (24) is used, where the superscripts "ref" and "approx" denote in this case the considered antenna parameter after the 1st (no coupling) and final iteration, respectively, and where the summations are taken over frequency samples. Hence, this table allows us to estimate how strong the feed-reflector coupling is and how it affects the antenna characteristics. As expected, the high-scattering horn feeds cause stronger multiscattering effects, which is further excercebated for smaller dishes due to the larger relative blockage area. The difference in the antenna characteristics and their ripples are largest for the case of the 38λ reflector fed by the horn with extended ground plane, while these values are comparable and weakly dependent on the antenna element type in case of the array feeds.

Table IV shows the mean values of various antenna radiation characteristics as well as their ripple caused by the multiscattering phenomenon, where the reflector antenna is assumed to be pointed at zenith for the computation of the spillover noise temperature T_{sp}. Upon comparing the values in the table, one conludes that the spillover noise temperature T_{sp} is most sensitive to the feed-reflector coupling, which may be of importance in radio astronomy applications where high receiving sensitivity is required.

Fig. 12 shows the illumination efficiencies η_{ill} of a 118λ reflector antenna ($D = 25$ m, $F/D = 0.35$), either fed by the Vivaldi array feed, or a single horn antenna. The numerically computed results are compared to measurements at the Westerbork Synthesis Radio Telescope (WSRT) [4]. As one can see, the agreement is very good. In the simulations, the size of the ground plane has been chosen equal to the size of the feed cabin ($\approx 1\times 1$ m). The fact that η_{ill} is higher for the array feed than for the horn antenna nicely demonstrates the superior focal field sampling capabilities of dense phased array feeds. Furthermore, one can also observe a rather strong ripple in η_{ill} for the case of the horn feed with extended ground plane. This ripple is caused by the relatively high feed scattering of the reflector field.

V. CONCLUSIONS

An FFT-enhanced Plane Wave Spectrum (PWS) approach has been formulated in conjunction with the Characteristic Basis Function Method, a Jacobi iterative multiscattering approach, and a near-field interpolation technique for the fast and accurate analysis of electrically large array feed reflector systems. Numerical validation has been carried out using the multilevel fast multipole algorithm method available in the commercially available FEKO software.

This physics-based numerical modeling offers the possibility to pull the feed-reflector interaction effects apart in a systematic manner and has demonstrated that: (i) a relation exists between the number of Jacobi iterations and the magnitude of the ripple on the frequency-dependent antenna radiation characteristics introduced by the feed-reflector coupling; (ii) the on-axis plane wave of the reflector field and the ones originating from the reflector rim are the strongest PWS components; (iii) the reflector-feed-induced ripple reduces when the array port termination is near a power-matched situation; (iv) the array feeds demonstrate a higher illumination efficiency than a single-horn feed with extended ground plane as a result of a better synthesized illumination pattern, and; (v) the level of the ripple as a function of frequency is smaller due to a smaller fraction of the scattered field from the array feed. The latter two findings have also been observed in measurements [4] for a horn feed and a 121-element Vivaldi PAF system installed at the Westerbork Synthesis Radio Telescope (118λ-diameter), where we have shown that the relative difference between the simulated and measured antenna efficiencies is only in the order of a few percent.

ACKNOWLEDGMENT

The authors thank Wim van Cappellen from ASTRON for providing the measurement data of the APERTIF PAF system.

REFERENCES

[1] B. Veidt. (2006) SKA memo 71: Focal-plane array architectures: Horn clusters vs. phased array techniques. [Online]. Available: http://www.skatelescope.org/uploaded/29162_71_Veidt.pdf

[2] M. V. Ivashina and C. G. M. van't Klooster, "Focal fields in reflector antennas and associated array feed synthesis for high efficiency multi-beam performances," in *Proc. 25th ESA Workshop on Satellite Antenna Technologies*, Noordwijk, The Netherlands, Sep. 2002, pp. 339–346.

[3] D. R. DeBoer, R. G. Gough, J. D. Bunton, T. J. Cornwell, R. J. Beresford, S. Johnston, I. J. Feain, A. E. Schinckel, C. A. Jackson, M. J. Kesteven, A. Chippendale, G. A. Hampson, J. D. O'Sullivan, S. G. Hay, C. E. Jacka, T. W. Sweetnam, M. C. Storey, L. Ball, and B. J. Boyle, "Australian SKA pathfinder: A high-dynamic range wide-field of view survey telescope," *Proc. IEEE*, vol. 97, no. 8, pp. 1507–1521, Aug. 2009.

[4] W. A. van Cappellen and L. Bakker, "APERTIF: Phased array feeds for the Westerbork synthesis radio telescope," in *IEEE International Symposium on Proc. Phased Array Systems and Technology (ARRAY)*, Boston, Oct. 2010, pp. 640–647.

[5] K. F. Warnick, "High efficiency phased array feed antennas for large radio telescopes and small satellite communication terminals," in *Proc. European Conference on Antennas and Propag. (EuCAP)*, Gothenburg, Sweden, Apr. 2013, pp. 448–449.

[6] O. A. Iupikov, M. V. Ivashina, K. Pontoppidan, P. H. Nielsen, C. Cappellin, N. Skou, S. S. Søbjærg, A. Ihle, D. Hartmann, and K. v. t Klooster, "Dense focal plane arrays for pushbroom satellite radiometers," in *Proc. European Conference on Antennas and Propag. (EuCAP)*, Hague, The Netherlands, Apr. 2014, pp. 1–5.

[7] P.-S. Kildal, "Factorization of the feed efficiency of paraboloids and cassegrain antennas," *IEEE Trans. Antennas Propag.*, vol. 33, no. 8, pp. 903–908, Aug. 1985.

[8] N. M. Kehn, M. V. Ivashina, P.-S. Kildal, and R. Maaskant, "Definition of unifying decoupling efficiency of different array antennas – case study of dense focal plane array feed for parabolic reflector," *Int. J. Electron. Commun. (AEU)*, doi: 10.1016/j.aeue.2009.02.011.

[9] M. V. Ivashina, M. Kehn, P.-S. Kildal, and R. Maaskant, "Decoupling efficiency of a wideband Vivaldi focal plane array feeding a reflector antenna," *IEEE Trans. Antennas Propag.*, vol. 57, no. 2, pp. 373–382, Feb. 2009.

[10] A. Moldsvor and P.-S. Kildal, "Systematic approach to control feed scattering and multiple reflections in symmetrical primary-fed reflector antennas," *IEEE Trans. Antennas Propag.*, vol. 139, no. 1, pp. 65–71, Sep. 1992.

[11] P.-S. Kildal, S. Skyttemyr, and A. Kishk, "G/T maximization of a paraboloidal reflector fed by a dipole-disk antenna with ring by using the multiple-reflection approach and the moment method," *IEEE Trans. Antennas Propag.*, vol. 45, no. 7, pp. 1130–1139, Jul. 1997.

[12] S. G. Hay, J. D. O'Sullivan, and R. Mittra, "Connected patch array analysis using the characteristic basis function method," *IEEE Trans. Antennas Propag.*, vol. 59, no. 6, pp. 1828–1837, Jun. 2011.

[13] R. Maaskant, M. V. Ivashina, O. Iupikov, E. A. Redkina, S. Kasturi, and D. H. Schaubert, "Analysis of large microstrip-fed tapered slot antenna arrays by combining electrodynamic and quasi-static field models," *IEEE Trans. Antennas Propag.*, vol. 56, no. 6, pp. 1798–1807, Jun. 2011.

[14] A. Popping and R. Braun, "The standing wave phenomenon in radio telescopes, frequency modulation of the wsrt primary beam," *Astronomy and Astrophysics*, vol. 479, no. 3, pp. 903–913, Mar. 2008.

[15] M. A. Apeldoorn. (2011) M.sc. thesis: Characterizing reflector-feed interaction for parabolic reflector antennas. [Online]. Available: http://repository.tudelft.nl/view/ir/uuid%3Ad6605869-37e0-49a6-8bc4-817855ab3710/MSc-Thesis-MAApeldoorn.pdf

[16] S. Hay, R. Mittra, and N. Huang. (2010) Analysis of reflector and feed scattering and coupling effects on the sensitivity of phased array feeds. [Online]. Available: http://csas.ee.byu.edu/docs/Workshop/BYU SGH.pdf

[17] W. A. van Cappellen and L. Bakker. (2010) Eliminating sensitivity ripples in prime focus reflectors with low-scattering phased array feeds. [Online]. Available: http://csas.ee.byu.edu/docs/Workshop/BYU_StandingWaves_Cappellen.pdf

[18] O. Iupikov, R. Maaskant, and M. Ivashina, "Towards the understanding of the interaction effects between reflector antennas and phased array feeds," in *Proc. Int. Conf. on Electromagn. in Adv. Applicat. (ICEAA)*, Cape Town, Sep. 2012, pp. 792–795.

[19] B. A. Munk, *Finite Antenna Arrays and FSS*. Danvers, Massachusetts: John Wiley & Sons, Inc., 2003.

[20] N.-T. Huang, R. Mittra, M. V. Ivashina, and R. Maaskant, "Numerical study of a dual-polarized focal plane array (FPA) with vivaldi elements in the vicinity of a large feed box using the parallelized FDTD code GEMS." in *Proc. IEEE AP-S International Symposium*, Charleston, USA, Jun. 2009, pp. 1522–3965.

[21] P. Bolli, G. Gentili, L. Lucci, R. Nesti, G. Pelosi, and G. Toso, "A hybrid perturbative technique to characterize the coupling between a corrugated horn and a reflector dish," *IEEE Trans. Antennas Propag.*, vol. 54, no. 2, pp. 595–603, Sep. 2006.

[22] M. Bandinelli, F. Milani, G. Guida, M. Bercigli, P. Frandsen, S. Sorensen, B. Bencivenga, and M. Sabbadini, "Feed-array design in presence of strong scattering from reflectors," in *Proc. European Conference on Antennas and Propag. (EuCAP)*, Rome, Italy, Apr. 2011, pp. 3844–3848.

[23] C. D. Giovampaola, E. Martini, A. Toccafondi, and S. Maci, "A hybrid PO/generalized-scattering-matrix approach for estimating the reflector induced mismatch," *IEEE Trans. Antennas Propag.*, vol. 60, no. 9, pp. 4316–4325, Sep. 2012.

[24] R. E. Hodges and Y. Rahmat-Samii, "An iterative current-based hybrid method for complex structures," *IEEE Trans. Antennas Propag.*, vol. 45, no. 2, pp. 265–276, Feb. 1997.

[25] C. S. Kim and Y. Rahmat-Samii, "Low profile antenna study using the physical optics hybrid method (POHM)," in *Proc. IEEE AP-S International Symposium*, Ontario, Canada, Jun. 1991, pp. 1350–1353.

[26] J. M. Taboada and F. Obelleiro, "Including multibounce effects in the moment-method physical-optics (MMPO) method," *Micr. Opt. Technol.*, vol. 32, no. 6, pp. 435–439, 2002.

[27] U. Jakobus and F. M. Landstorfer, "Improved PO-MM hybrid formulation for scattering from three-dimensional perfectly conducting bodies of arbitrary shape," *IEEE Trans. Antennas Propag.*, vol. 43, no. 2, pp. 162–169, Feb. 1995.

[28] B. Andres-Garcia, D. Gonzalez-Ovejero, C. Craeye, L. Garcia-Muoz, and D. Segovia-Vargas, "An iterative MoM-PO method based on a MBF/Krylov approach," in *Proc. European Conference on Antennas and Propag. (EuCAP)*, Barcelona, Spain, Apr. 2010, pp. 1–4.

[29] W. A. van Cappellen, L. Bakker, and T. A. Oosterloo, "Experimental results of the APERTIF phased array feed," in *General Assembly and Scientific Symposium, 2011 XXXth URSI*, Istanbul, Turkey, Aug. 2011, pp. 1–4.

[30] Y. Brand, A. K. Skrivervik, J. R. Mosig, and F. E. Gardiol, "New iterative integral equation technique for multilayered printed array antennas," in *Mathematical Methods in Electromagnetic Theory*, Kharkov, Ukraine, Jun. 1998, pp. 615–617.

[31] A. C. Polycarpou, "Evaluation of stationary block iterative techniques for the solution of finite arrays using the FE-BI method and domain

decomposition," in *Proc. European Conference on Antennas and Propag. (EuCAP)*, Nice, France, Nov. 2006, pp. 1–6.
[32] S. N. Makarov, *Antenna and EM Modeling With MATLAB*. New York: John Wiley and Sons, Inc., 2002.
[33] R. Maaskant, "Analysis of large antenna systems," Ph.D. dissertation, Eindhoven University of Technology, Eindhoven, 2010. [Online]. Available: http://alexandria.tue.nl/extra2/201010409.pdf
[34] P.-S. Kildal, *Foundations of Antennas: a Unified Approach*. Lund: Studentlitteratur, 2000.
[35] C. A. Balanis, *Advanced Engineering Electromagnetics*. New York: John Wiley and Sons, Inc., 1989.
[36] R. Maaskant, R. Mittra, and A. G. Tijhuis, "Fast analysis of large antenna arrays using the characteristic basis function method and the adaptive cross approximation algorithm," *IEEE Trans. Antennas Propag.*, vol. 56, no. 11, pp. 3440–3451, Nov. 2008.
[37] O. A. Iupikov, R. Maaskant, and M. V. Ivashina, "A plane wave approximation in the computation of multiscattering effects in reflector systems," in *Proc. European Conference on Antennas and Propag. (EuCAP)*, Gothenburg, Sweden, Apr. 2013, pp. 3828–3832.
[38] J. J. H. Wang, "An examination of the theory and practices of planar near-field measurement," *IEEE Trans. Antennas Propag.*, vol. 36, no. 6, pp. 746–753, Jun. 1988.
[39] J. P. McKay and Y. Rahmat-Samii, "Compact range reflector analysis using the plane wave spectrum approach with an adjustable sampling rate," *IEEE Trans. Antennas Propag.*, vol. 39, no. 6, pp. 746–753, Jun. 1991.
[40] R. C. Rudduck, D. C. Wu, and M. Intihar, "Near-field analysis by the plane-wave spectrum approach," *IEEE Trans. Antennas Propag.*, vol. 21, no. 2, pp. 231–234, Mar. 1973.
[41] (2007) EM Software & Systems – S.A. (Pty) Ltd, Stellenbosch, South Africa, FEKO, Suite 6.0. [Online]. Available: http://www.feko.info
[42] M. Arts, M. Ivashina, O. Iupikov, L. Bakker, and R. van den Brink, "Design of a low-loss low-noise tapered slot phased array feed for reflector antennas," in *Proc. European Conference on Antennas and Propag. (EuCAP)*, Barcelona, Spain, Apr. 2010, pp. 1–5.
[43] M. V. Ivashina, R. Maaskant, and B. Woestenburg, "Equivalent system representation to model the beam sensitivity of receiving antenna arrays," *IEEE Antennas Wireless Propag. Lett.*, vol. 7, no. 1, pp. 733–737, Jan. 2008.

Oleg Iupikov received a MSc degree (*cum laude*) in Electrical Engineering in 2006, from the Sevastopol National Technical University, Ukraine. After graduating, he was working at the Radio Engineering Bureau, Sevastopol. During this period, he was also a visiting scientist at The Netherlands Institute for Radio Astronomy (ASTRON), where he was involved in the development of the focal plane array simulation software for the APERTIF radio telescope. This visit was funded by the SKADS Marie Curie visitor grant and the APERTIF project. From November 2011, he is a PhD student at the Antenna Group of Chalmers University of Technology, Sweden. His PhD project is devoted to the development of numerical methods for optimization of focal plane array systems and their efficient calibration in the context of the next generation radio telescope known as the Square Kilometre Array (SKA).

Rob Maaskant (M'11-SM'13) received his M.Sc. degree (*cum laude*) in 2003, and his Ph.D. degree (*cum laude*) in 2010, both in Electrical Engineering from the Eindhoven University of Technology, Eindhoven, The Netherlands. His Ph.D. has been awarded "the best dissertation of the Electrical Engineering Department, 2010." From 2003–2010, he was employed as an antenna research scientist at the Netherlands Institute for Radio Astronomy (ASTRON), Dwingeloo, The Netherlands, and from 2010–2012 as a postdoctoral researcher in the Antenna Group of the Signals and Systems Department at the Chalmers University of Technology, Sweden, for which he won a European Commission FP7 Marie Sklodowska-Curie Actions Outgoing – Rubicon Fellowship from the Netherlands Organization for Scientific Research (NWO), 2010. He is currently an Assistant Professor in the same Antenna Group. He is the primary author of the CAESAR software; an advanced integral-equation based solver for the analysis of large antenna array systems. His current research interest is in the field of receiving antennas for low-noise applications, meta-material based waveguides, and computational electromagnetics to solve these types of problems.

Dr. Maaskant received the 2nd best paper prize ('best team contribution') at the 2008 ESA/ESTEC workshop, Noordwijk, and was awarded a Young Researcher grant from the Swedish Research Council (VR), in 2011. He is an Associate Editor of both the IEEE Transactions on Antennas and Propagation and the FERMAT journal.

Marianna V. Ivashina (M'11-SM'13) received a Ph.D. in Electrical Engineering from the Sevastopol National Technical University (SNTU), Ukraine, in 2000. From 2001 to 2004 she was a Postdoctoral Researcher and from 2004 till 2010 an Antenna System Scientist at The Netherlands Institute for Radio Astronomy (ASTRON). During this period, she carried out research on an innovative Phased Array Feed (PAF) technology for a new-generation radio telescope, known as the Square Kilometer Array (SKA). The results of these early PAF projects have led to the definition of APERTIF - a PAF system that is being developed at ASTRON to replace the current horn feeds in the Westerbork Synthesis Radio Telescope (WSRT). Dr. Ivashina was involved in the development of APERTIF during 2008-2010 and acted as an external reviewer at the Preliminary Design Review of the Australian SKA Pathfinder (ASKAP) in 2009. In 2002, she also stayed as a Visiting Scientist with the European Space Agency (ESA), ESTEC, in the Netherlands, where she studied multiple-beam array feeds for the satellite telecommunication system Large Deployable Antenna (LDA). Dr. Ivashina received the URSI Young Scientists Award for the GA URSI, Toronto, Canada (1999), an APS/IEEE Travel Grant, Davos, Switzerland (2000), the 2nd Best Paper Award ('Best team contribution') at the ESA Antenna Workshop (2008) and the International Qualification Fellowship of the VINNOVA - Marie Curie Actions Program (2009) and The VR project grant of the Swedish Research Center (2010). She is currently an Associate Professor at the Department of Signals and Systems (Chalmers University of Technology). Her interests are wideband receiving arrays, antenna system modeling techniques, receiver noise characterization, signal processing for phased arrays, and radio astronomy. She is an Associate Editor of the IEEE Transactions on Antennas and Propagation and the FERMAT journal.

André Young (S'13-M'14) was born in the Free State, South Africa on April 6, 1983. He received the B.Eng. degree in electrical and electronic engineering with computer science (*cum laude*), the M.Sc.Eng. degree in electronic engineering (*cum laude*), and PhD in electronic engineering in 2005, 2007, and 2013, respectively, from the University of Stellenbosch, Stellenbosch, South Africa. His doctoral thesis was on improving the direction-dependent gain calibration of reflector antenna radio telescopes.

He has worked on various engineering projects for Azoteq (Paarl, South Africa) and Entersekt (Stellenbosch, South Africa), and is currently appointed as a post-doctoral associate at Stellenbosch University, where he was also appointed as a Junior Lecturer in 2009 and 2011. Since 2011 he has spent several months as a visiting researcher with the Antenna Group at the Chalmers University of Technology, Gothenburg, Sweden. His main research interests include computational electromagnetics and antennas.

Per-Simon Kildal (M'76-SM'81-F'95) is professor in antennas at Chalmers University of Technology in Gothenburg, Sweden since 1989. He is heading the Antenna group. His main tasks are to lead and supervise research within antenna systems. Until now, 19 persons have received a Ph.D. from him. Kildal received himself two doctoral degrees from the Norwegian Institute of Technology in Trondheim. Kildal has authored more than 120 articles in scientific journals; concerning antenna theory, analysis, design and measurements. Two articles were awarded best paper awards by IEEE (1985 R.W.P. King Award and 1991 Schelkunoff Prize Paper Award). In 2011 he received the prestigious Distinguished Achievements Award from the IEEE Antennas and Propagation Society.

Kildal has done the electrical design of the 40 m $\times$120 m cylindrical reflector antenna and line feed of the EISCAT scientific organization, and the dual-reflector Gregorian feed of the 300 m radio telescope in Arecibo. He is the inventor behind technologies such as dipole with beam forming ring, the hat antenna, and the eleven feed. All these feeds have been used in industry, and until now more than 930 000 hat-fed reflectors have been manufactured for use in radio links. Kildal was the first to introduce the reverberation chamber as an accurate measurement instrument for Over-The-Air (OTA) characterization of small antennas and wireless terminals for use in multipath environments with fading. Kildal is also the originator of the concept of soft and hard surfaces from 1988, today being regarded as the first metamaterials concept. This concept is the basis of his newest and most fundamental invention, the gap waveguide technology. His research is innovative and industrially oriented, and has resulted in several patents and related spinoff companies, the most known being Bluetest AB.

Kildal organizes and lectures in courses within the *European School of Antenna* (ESoA, www.antennasvce.org). His textbook *Foundations of Antennas - A Unified Approach* (Lund, Sweden: Studentlitteratur, 2000) was well received, and is now in the process of being revised.